ELSEVIER

Journal of Biomechanics 41 (2008) 447–453

JOURNAL OF BIOMECHANICS

www.elsevier.com/locate/jbiomech
www.JBiomech.com

Prediction of arterial failure based on a microstructural bi-layer fiber–matrix model with softening

K.Y. Volokh*

Faculty of Civil and Environmental Engineering, Technion-I.I.T., Haifa 32000, Israel

Accepted 8 August 2007

Abstract

Two approaches to predict failure of soft tissue are available. The first is based on a pointwise criticality condition, e.g. von Mises maximum stress, which is restrictive because only local state of deformation is considered to be critical and the failure criterion is separated from stress analysis. The second is based on damage mechanics where internal (unobservable) variables are introduced which make the experimental calibration of the theory complex. As an alternative to the local failure criteria and damage mechanics we present a softening hyperelasticity approach, where the constitutive description of soft tissue is enhanced with strain softening, which is controlled by material constants. This approach is attractive because the new material constants can be readily calibrated in experiments on the one hand and the failure criteria are global on the other hand. We illustrate the efficiency of the softening hyperelasticity approach on the problem of prediction of arterial failure. For this purpose, we enhance a bi-layer fiber–matrix microstructural arterial model with softening and analyze the arterial failure under internal pressure. We show that the overall arterial strength is (a) dominated by the media layer, (b) controlled by microfibers and (c) increased by residual stresses.

Keywords: Artery; Fiber; Failure; Hyperelasticity; Softening

1. Introduction

Enormous progress has been made in phenomenological modeling of soft tissue: (Fung, 1993; Humphrey, 2002; Cowin and Humphrey, 2002; Holzapfel and Ogden, 2003, 2006). Some issues, nonetheless, require further elaboration. Among them is a theoretical description of tissue failure. Two approaches to predict failure of soft tissue are available. The first—strength of materials—approach is based on a pointwise criticality condition. According to it, material/structure failure is claimed when, for example, the maximum von Mises stress at a point reaches a critical value. Evidently, such an approach is restrictive because the local state of deformation defines global failure, which is not necessarily correct. Moreover, the critical value of the von Misses stress is defined separately from stress analysis. The drawbacks of the first approach do not exist in the second—damage mechanics—approach that allows modeling global failure and includes the failure condition in its constitutive description. In damage mechanics, a scalar or tensor parameter is introduced to describe the degradation of material properties during mechanical loading (Hurschler et al., 1997; Hokanson and Yazdami, 1997; Liao and Belkoff, 1999; Arnoux et al., 2002; Schechtman and Bader, 2002; Natali et al., 2005; Rodriguez et al., 2006; Calvo et al., 2006). The damage parameter is an internal variable whose magnitude is constrained by (a) a damage evolution equation and (b) a critical threshold condition. Theoretically, the approach of damage mechanics is very flexible and allows reflecting the physical processes triggering macroscopic damage at small length scales. Practically, the experimental calibration of damage theories is far from trivial and, because of that, it is reasonable to look for alternative theories that present the bulk failure in more feasible ways than the traditional damage theories.

As an alternative to the simplistic description of strength of materials on the one hand and the sophisticated approach of damage mechanics on the other hand we

*Tel.: +972 48292426.
E-mail address: cvolokh@tx.technion.ac.il

0021-9290/$ - see front matter © 2007 Elsevier Ltd. All rights reserved.
doi:10.1016/j.jbiomech.2007.08.001

present a softening hyperelasticity approach, where the constitutive description of soft tissue is enhanced with strain softening, which is controlled by material constants. The novel approach is attractive because the new material constants can be readily calibrated in experiments and the failure description is included in the constitutive law. We illustrate the efficiency of the softening hyperelasticity approach on the problem of the prediction of arterial failure. For this purpose, we enhance the earlier bi-layer fiber-reinforced arterial model with softening and analyze the arterial failure under internal pressure.

2. Methods

2.1. Constitutive model of the intact arterial wall

Histological analysis of the arterial wall (Humphrey, 2002; Holzapfel and Ogden, 2003) reveals that the artery comprises three layers—intima, media, and adventitia. While the mechanical role of intima is minor, the media and adventitia contribute to the arterial strength. Both media and adventitia are anisotropic composite materials reinforced with a net of oriented collagen fibers. There are a number of constitutive theories presenting passive behavior of arteries which include material anisotropy (Vaishnav et al., 1973; Fung et al., 1979; von Maltzahn et al., 1981; Chuong and Fung, 1983; Tözeren, 1984; Demiray, 1991; Humphrey, 1995; Wuyts et al., 1995; Delfino et al., 1997; Simon et al., 1998a, b). We choose the latest and most complicated theory proposed by Holzapfel et al. (2000) to account for the bi-layer structure of the artery, where both adventitia and media are fiber-reinforced composites.

We start with the classical formulation of continuum mechanics according to which a generic material particle of body Ω occupying position $\mathbf{X}$ at the reference state moves to position $\mathbf{x}(\mathbf{X})$ in the current configuration. The deformation of the particle is defined by the tensor of deformation gradient $\mathbf{F}=\partial\mathbf{x}/\partial\mathbf{X}$. The equilibrium equation and boundary conditions are set in the form

$$\mathrm{div}\boldsymbol{\sigma}=0 \text{ in } \Omega, \tag{1}$$

$$\mathbf{x}=\bar{\mathbf{x}} \text{ on } \partial\Omega_{\mathbf{x}} \text{ or } \boldsymbol{\sigma}\mathbf{n}=\bar{\mathbf{t}} \text{ on } \partial\Omega_{\mathbf{t}}, \tag{2}$$

where 'div' operator is with respect to the current coordinates; $\boldsymbol{\sigma}$ is the Cauchy stress tensor; $\mathbf{t}$ is traction per unit area of the current surface with the unit outward normal $\mathbf{n}$. The barred quantities are prescribed.

We assume that material is incompressible in all subsequent considerations

$$\det\mathbf{F}=1. \tag{3}$$

Such an assumption is often used for analysis of soft biological materials because their response to hydrostatic pressure is much stronger than their response to shearing. It seems, however, that the applicability of the incompressibility assumption essentially depends on the specific loading and deformation of the material under consideration (Volokh, 2006a).

Holzapfel Gasser and Ogden (2000) suggest writing the constitutive equations for the adventitia or media in the following form:

$$\boldsymbol{\sigma}=\boldsymbol{\sigma}^{M}+\boldsymbol{\sigma}^{F_1}+\boldsymbol{\sigma}^{F_2}, \tag{4}$$

$$\boldsymbol{\sigma}^{M}=-p\mathbf{1}+2W_1\mathbf{B}, \tag{5}$$

$$\boldsymbol{\sigma}^{F_1}=2V_1\mathbf{m}_1\otimes\mathbf{m}_1, \tag{6}$$

$$\boldsymbol{\sigma}^{F_2}=2V_2\mathbf{m}_2\otimes\mathbf{m}_2, \tag{7}$$

$$W_1\equiv\partial W/\partial I_1; \quad V_i\equiv\partial V/\partial J_i. \tag{8}$$

Here the Cauchy stress tensor is decomposed into $\boldsymbol{\sigma}^{M}$ representing the arterial matrix and $\boldsymbol{\sigma}^{F_1}$ and $\boldsymbol{\sigma}^{F_2}$ representing two families of fibers; p is the Lagrange multiplier enforcing the incompressibility condition (3); $\mathbf{1}$ is the second order identity tensor; $W(I_1)$ is a stored elastic energy of the arterial matrix per unit reference volume defined as a function of the first principal invariant of the left $\mathbf{B}=\mathbf{F}\mathbf{F}^{\mathrm{T}}$ Cauchy–Green deformation tensor: $I_1=\mathrm{tr}\,\mathbf{B}$; vectors $\mathbf{m}_i=\mathbf{F}\mathbf{M}_i$ designate 'pushed forward' initial fiber directions $\mathbf{M}_i$ ($|\mathbf{M}_i|=1$); and $V(J_1, J_2)$ is a stored elastic energy of the stretching fibers: $J_i=\mathbf{m}_i\cdot\mathbf{m}_i$.

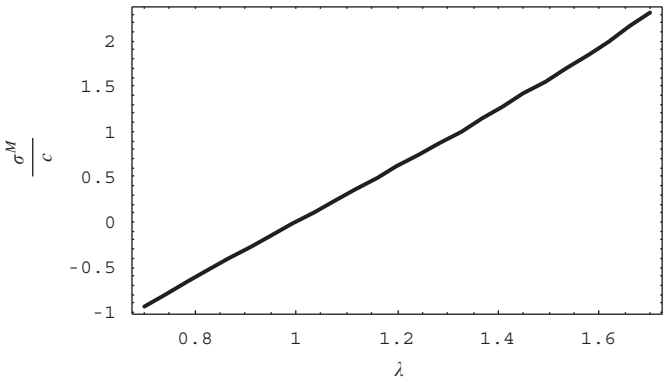

Fig. 1. Neo–Hookean matrix material in uniaxial tension.

The matrix material is Neo–Hookean

$$W(I_1)=\frac{c}{2}(I_1-3), \tag{9}$$

while the fibers are described by the exponential stored energy

$$V(J_1,J_2)=\frac{k_1}{2k_2}\{\exp(k_2(J_1-1)^2)+\exp(k_2(J_2-1)^2)-2\}. \tag{10}$$

Substituting (9) and (10) in (8) we have

$$W_1=\frac{c}{2}, \tag{11}$$

$$V_i=k_1(J_i-1)\exp(k_2(J_i-1)^2). \tag{12}$$

In the case of the uniaxial tension of the matrix material (without fibers) the deformation can be described as follows:

$$x_1=\lambda X_1; \quad x_2=\lambda^{-1/2}X_2; \quad x_3=\lambda^{-1/2}X_3. \tag{13}$$

Based on (5) we find [1] (Fig. 1)

$$\sigma^{M}\equiv\sigma^{M}_{11}=2W_1(\lambda^2-\lambda^{-1})=c(\lambda^2-\lambda^{-1}). \tag{14}$$

In the case of tension of an individual fiber we have $\mathbf{m}_i=\lambda\mathbf{M}_i\Rightarrow J_i=\lambda^2$ and, consequently, (Fig. 2)

$$\sigma^{F_i}\equiv\mathbf{m}\cdot\boldsymbol{\sigma}^{F_i}\mathbf{m}/(\mathbf{m}\cdot\mathbf{m})=2V_i\lambda^2=2k_1(\lambda^2-1)\lambda^2\exp\{k_2(\lambda^2-1)^2\}. \tag{15}$$

We will use (14) and (15) for the calibration of the softening hyperelasticity model in the next section.

2.2. Constitutive model of the arterial wall with failure

The idea to include intrinsic softening in the phenomenological description of material failure appears in Volokh (2004, 2007a), where it is applied to quasibrittle materials undergoing small deformations. Below we extend the softening hyperelasticity approach to the arterial model which allows for large deformations and strains.

We introduce a softening Neo–Hookean model for the matrix material as follows:

$$W(I_1)=\phi-\phi\exp\left\{-\frac{c}{2\phi}(I_1-3)\right\}. \tag{16}$$

[1] This is a particular case of the celebrated Rivlin's, (1948) solution.

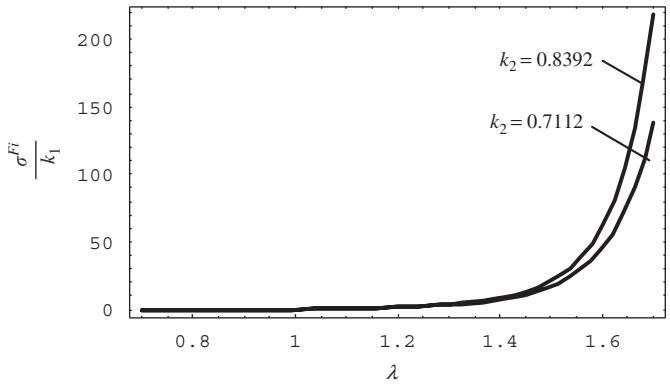

Fig. 2. Fiber in tension.

Constant ϕ designates the maximum work which material can undergo before failure. Indeed, putting $I_1 \to \infty$, i.e. considering the tension dominated deformation, we get $W(\infty) = \phi$. Thus ϕ is a material failure work which is a material constant. This is in contrast to the traditional Neo–Hookean material where the work on deformation is unlimited $W(\infty) = \infty$. The latter is unphysical, of course, because no real material can sustain large enough deformations without failure. It should be noted that the linearized version of (16) presents the classical Neo–Hookean material.

Fig. 3 demonstrates the qualitative difference between the classical Neo–Hookean material without softening—(9)—and the one with softening—(16).

Differentiating (16) with respect to the first principal invariant we get

$$W_1 = \frac{c}{2}\exp\left\{-\frac{c}{2\phi}(I_1 - 3)\right\}. \tag{17}$$

In the case of uniaxial tension we have instead of (14)

$$\begin{aligned}\sigma^M \equiv \sigma^M_{11} &= 2(\lambda^2 - \lambda^{-1})W_1 \\ &= c(\lambda^2 - \lambda^{-1})\exp\left\{-\frac{c}{2\phi}(\lambda^2 + 2\lambda^{-1} - 3)\right\}.\end{aligned} \tag{18}$$

The load–stretch curves described by (14) and (18) are given in Fig. 4. The maximum point on the curve corresponding to the softening material indicates the onset of the material failure/rupture. After the stretch reaches the magnitude of ~1.8 no stable solution of the statical problem exists. All this is in perfect correspondence with our physical intuition and observation. Actually, the uniaxial tension test can be used for calibration of the material failure constant ϕ. Though we do not have the direct experiments to calibrate the matrix material, some qualitative comparison of the shape of the failure curve in Fig. 4 with the Raghavan and Vorp (2000) experimental data on the rupture of the abdominal aortic aneurism is encouraging.

We introduce the softening fiber model as follows:

$$\begin{aligned}V_i &= k_1(J_i - 1)\exp\{k_2(J_i - 1)^2 \\ &\quad - k_2(J_i - 1)^{2n_i}/(\xi_i^2 - 1)^{2n_i}\}.\end{aligned} \tag{19}$$

Now the fiber tension versus stretch (14) takes the form

$$\begin{aligned}\sigma^{Fi} &= 2V_i\lambda^2 \\ &= 2k_1(\lambda^2 - 1)\lambda^2\exp\{k_2(\lambda^2 - 1)^2 \\ &\quad - k_2(\lambda^2 - 1)^{2n_i}/(\xi_i^2 - 1)^{2n_i}\}.\end{aligned} \tag{20}$$

The graph of (20) with and without softening is presented in Fig. 5 for the media: $k_2 = 0.8392$; $\xi_i = 1.5$; $n_i = 2$ or 10.

It should not be missed that the fiber is defined by two failure constants ξ and n in contrast to the matrix material defined by only one failure constant ϕ. The second failure constant of the fiber, n, controls the 'sharpness' of the stress–strain curve as it is seen in Fig. 5.

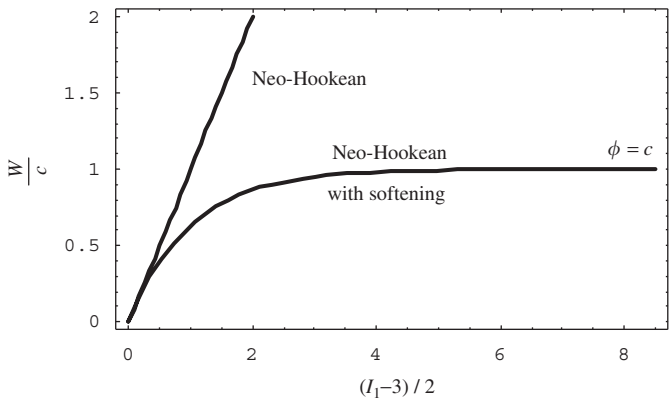

Fig. 3. The meaning of softening hyperelasticity: the energy approaches the limit failure state.

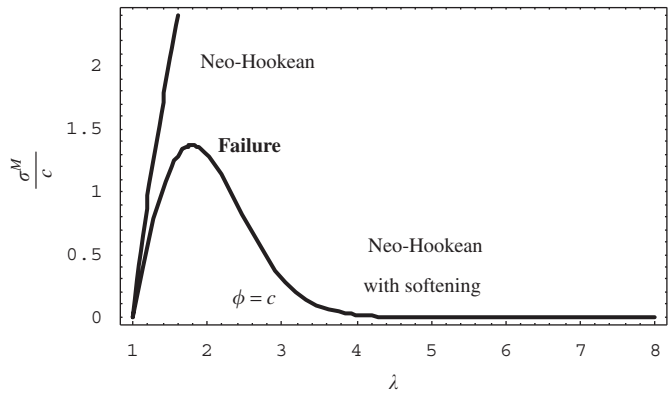

Fig. 4. Neo–Hookean matrix material with and without softening in uniaxial tension.

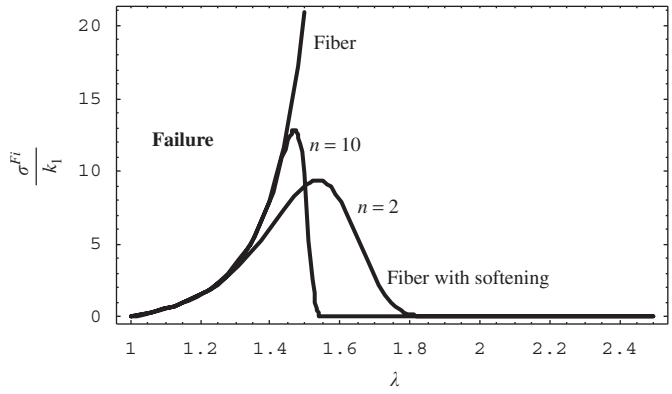

Fig. 5. Fiber material with and without softening in tension.

2.3. Artery inflation

In this section, we use the model with softening developed above for studying arterial failure under internal pressure. For this purpose, we consider the radial inflation of an artery as a symmetric deformation of a cylinder obeying the incompressibility conditions (Holzapfel et al., 2000)

$$r = \sqrt{\frac{R^2 - A^2}{\gamma s} + a^2}, \quad \theta = \gamma\Theta, \quad z = sZ, \tag{21}$$

where a point occupying position (R, Θ, Z) in the initial configuration is moving to position (r, θ, z) in the current configuration; s is the axial

stretch; $\gamma = 2\pi/(2\pi-\omega)$, where ω is the artery opening angle in the unstressed configuration; A and a are the internal artery radii before and after deformation accordingly. Then, the deformation gradient and the left Cauchy–Green deformation tensor take the following forms:

$$\mathbf{F} = (\gamma sr/R)^{-1}\mathbf{k}_r \otimes \mathbf{K}_R + (\gamma r/R)\mathbf{k}_\theta \otimes \mathbf{K}_\Theta + s\mathbf{k}_z \otimes \mathbf{K}_Z, \tag{22}$$

$$\mathbf{B} = (\gamma sr/R)^{-2}\mathbf{k}_r \otimes \mathbf{k}_r + (\gamma r/R)^2\mathbf{k}_\theta \otimes \mathbf{k}_\theta + s^2\mathbf{k}_z \otimes \mathbf{k}_z, \tag{23}$$

where $\{\mathbf{K}_R, \mathbf{K}_\Theta, \mathbf{K}_z\}$ and $\{\mathbf{k}_r, \mathbf{k}_\theta, \mathbf{k}_z\}$ are the orthonormal bases[2] in cylindrical coordinates at the reference and current configurations accordingly.

The fiber kinematics is described by

$$\mathbf{m}_1 = \mathbf{F}\mathbf{M}_1 = (\gamma r\cos\beta/R)\mathbf{k}_\theta + s(\sin\beta)\mathbf{k}_z, \tag{24}$$

$$\mathbf{m}_2 = \mathbf{F}\mathbf{M}_2 = (\gamma r\cos\beta/R)\mathbf{k}_\theta - s(\sin\beta)\mathbf{k}_z, \tag{25}$$

where the initial fiber directions are $\mathbf{M}_1 = \cos\beta\,\mathbf{K}_\Theta + \sin\beta\,\mathbf{K}_z$ and $\mathbf{M}_2 = \cos\beta\,\mathbf{K}_\Theta - \sin\beta\,\mathbf{K}_z$. Here β is the angle between the fibers and the circumferential direction of the artery.

Gathering all stress terms with the help of (4)–(7) and (23)–(25), we get the nontrivial components of the Cauchy stress

$$\begin{aligned}
\sigma_{rr} &= -p + 2W_1R^2/(\gamma sr)^2,\\
\sigma_{\theta\theta} &= -p + 2W_1(\gamma r/R)^2 + 2(V_1+V_2)(\gamma r\cos\beta/R)^2,\\
\sigma_{zz} &= -p + 2W_1s^2 + 2(V_1+V_2)(s\sin\beta)^2,\\
\sigma_{z\theta} &= \sigma_{\theta z} = 2(V_1-V_2)\gamma rs\cos\beta\sin\beta,
\end{aligned} \tag{26}$$

where W_1, V_1, V_2 are defined in (17) and (19) accordingly and the invariants take the form

$$\begin{aligned}
I_1 &= R^2/(\gamma sr)^2 + (\gamma r/R)^2 + s^2,\\
J_1 &= J_2 = (\gamma r\cos\beta/R)^2 + (s\sin\beta)^2.
\end{aligned} \tag{27}$$

We notice that the latter equation and the assumption $\xi_1 = \xi_2$ provide $V_1 = V_2$ and, consequently, $\sigma_{z\theta} = \sigma_{\theta z} = 0$.

In summary, there is only one nontrivial equilibrium equation

$$\frac{\partial\sigma_{rr}}{\partial r} + \frac{\sigma_{rr}-\sigma_{\theta\theta}}{r} = 0. \tag{28}$$

The traction boundary conditions are

$$\begin{aligned}
\sigma_{rr}(r=a) &= -g,\\
\sigma_{rr}(r=b) &= 0,
\end{aligned} \tag{29}$$

where b is the outer radius of the artery after the deformation, which was equal to B before the deformation.

We integrate equilibrium equation (28) over the wall thickness with account of boundary conditions (29) and get

$$\begin{aligned}
g(a) &= -\int_a^{b(a)}(\sigma_{rr}-\sigma_{\theta\theta})\frac{\mathrm{d}r}{r}\\
&= -\int_a^{b(a)}(2W_1R^2/(\gamma sr)^2 - 2W_1(\gamma r/R)^2 - 4V_1(\gamma r\cos\beta/R)^2)\frac{\mathrm{d}r}{r},
\end{aligned} \tag{30}$$

where $b(a) = \sqrt{a^2 + (B^2-A^2)/(\gamma s)}$.

Eq. (30) presents the pressure–radius (g–a) relationship, which we examine for various material constants in the next section. Before doing that, however, we introduce dimensionless variables as follows:

$$\bar{g} = \frac{g}{c};\quad \bar{r} = \frac{r}{A};\quad \bar{R} = \frac{R}{A}\quad \bar{a} = \frac{a}{A};\quad \bar{b} = \frac{b}{A}. \tag{31}$$

Now Eq. (30) takes form

$$\bar{g}(\bar{a}) = -\int_{\bar{a}}^{\bar{b}(\bar{a})}\Big(2\bar{W}_1\bar{R}^2/(\gamma s\bar{r})^2 - 2\bar{W}_1(\gamma\bar{r}/\bar{R})^2 - 4\bar{V}_1(\gamma\bar{r}\cos\beta/\bar{R})^2\Big)\frac{\mathrm{d}\bar{r}}{\bar{r}}, \tag{32}$$

where

$$\bar{b}(\bar{a}) = \sqrt{\bar{a}^2 + ((B/A)^2-1)/(\gamma s)}, \tag{33}$$

$$\bar{W}_1 = \frac{1}{2}\exp\left\{-\frac{c}{2\phi}(I_1-3)\right\}, \tag{34}$$

$$\bar{V}_1 = \frac{k_1}{c}(J_1-1)\exp\{k_2(J_1-1)^2 - k_2(J_1-1)^{2n_1}/(\xi_1^2-1)^{2n_1}\}, \tag{35}$$

$$I_1 = \bar{R}^2/(\gamma s\bar{r})^2 + (\gamma\bar{r}/\bar{R})^2 + s^2, \tag{36}$$

$$J_1 = (\gamma\bar{r}\cos\beta/\bar{R})^2 + (s\sin\beta)^2, \tag{37}$$

$$\bar{R}^2 = \gamma s(\bar{r}^2 - \bar{a}^2) + 1. \tag{38}$$

Remark 1. In the present work, we introduce residual stresses (Rachev and Greenwald, 2003) via the opening angle parameter, ω, in a stress-free configuration (Holzapfel et al., 2000). Residual stresses are one of the most intriguing features of mechanics of living tissues. While the qualitative nature of residual stresses related with tissue growth is understood reasonably well, the best way to quantify them remains to be settled (Volokh, 2006b).

Remark 2. The idea to account for the matrix material failure with the help of Eq. (16) is rather universal and can be applied to fibers as well as any hyperelastic material too (Volokh, 2007b). Nonetheless, we prefer a different description of fibers—(19)—because it adds flexibility to the account of the shape of the stress–strain curve. In particular, formula (19) with large n allows for the account of the abrupt rupture of fibers observed in experiments and molecular dynamic simulations (Buehler, 2006; Kabla and Mahadevan, 2007).

Remark 3. It should not be missed that material constants change from the media to adventitia and, thus, the integral in Eq. (32) should be split in computations in two integrals for the media and adventitia accordingly.

3. Results

The purpose of numerical simulations is twofold. First, we aim at clarifying the relative importance of matrix and fibers within the media layer[3] of the arterial wall. Second, we examine the comparative contribution of the adventitia and media in the overall arterial strength as well as the influence of residual stresses.

We use Mathematica (Wolfram, 2003) for the numerical integration of Eq. (32).

As a 'ground state' of material constants, which will vary in calculations, we choose the parameters reported by Holzapfel et al. (2000) for the media: $c_M = 3.0\,\mathrm{KPa}$, $k_{1M} = 2.36\,\mathrm{KPa}$, $k_{2M} = 0.84$, $A = 0.7\,\mathrm{mm}$, $B_M = 0.96\,\mathrm{mm}$, $\beta_M = \pi/6$; and for the adventitia: $c_A = 3.0\,\mathrm{KPa}$,

[2] $\mathbf{K}_R = (\cos\Theta, \sin\Theta, 0)^{\mathrm{T}}$; $\mathbf{K}_\Theta = (-\sin\Theta, \cos\Theta, 0)^{\mathrm{T}}$; $\mathbf{K}_Z = (0,0,1)^{\mathrm{T}}$; $\mathbf{k}_r = (\cos\theta, \sin\theta, 0)^{\mathrm{T}}$; $\mathbf{k}_\theta = (-\sin\theta, \cos\theta, 0)^{\mathrm{T}}$; $\mathbf{k}_z = (0,0,1)^{\mathrm{T}}$.

[3] We choose the media because it is stiffer than the adventitia.

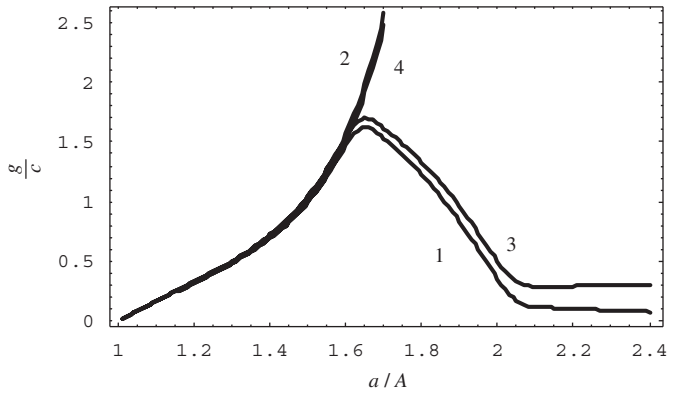

Fig. 6. Pressure–displacement curve for the 'ground state' of the inflating media: matrix and fibers with softening, 1; matrix and fibers without softening, 2; fibers with and matrix without softening, 3; matrix with and fibers without softening, 4.

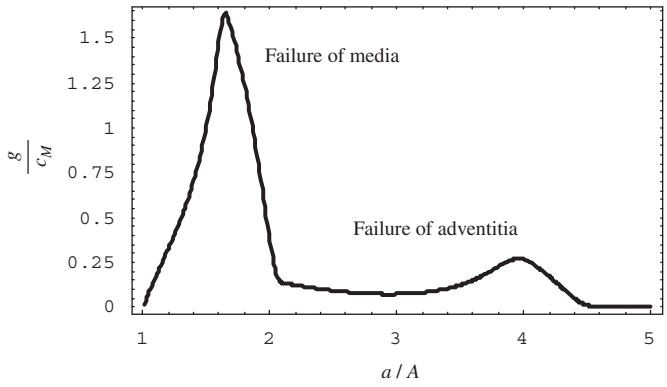

Fig. 7. Pressure–displacement curve for the 'ground state' of the bi-layer arterial wall model.

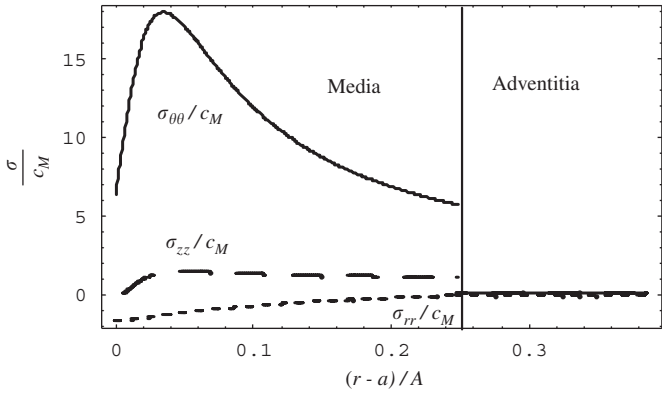

Fig. 8. Distribution of the Cauchy stresses at the point of the media rupture.

$k_{1A} = 0.56\,\mathrm{KPa}$, $k_{2A} = 0.7112$, $A_A = B_M$, $B = 1.09\,\mathrm{mm}$, $\beta_A = \pi/3$. These parameters were fitted to the experimental data of Chuong and Fung (1983) for a carotid artery of a rabbit. We complete the softening hyperelastic model with material constants controlling failure of the media and the adventitia accordingly: $\phi_M = c_M$, $\xi_{1M} = 1.5$, $n_{1M} = 10$ and $\phi_A = c_A$, $\xi_{1A} = 1.7$, $n_{1A} = 10$. Besides, we assume $s = 1$ and $\omega = 0$, there is no axial stretch and residual stress.

The pressure–displacement curve #1 in Fig. 6 presents the media failure for the ground state described above. In this case the softening is allowed for both matrix and fibers. The media without softening is presented by curve #2. The case where the matrix does not soften while the fibers do is presented by curve #3 and the case where the fibers do not soften while the matrix does is presented by curve #4. It is readily observed in Fig. 6 that *the overall strength is controlled by the strength of the fibers*. Indeed, when the fibers soften the media softens and when the fibers do not the media does not.

Further, we examined the effect of a ten times decrease $k_{1M} = 0.236\,\mathrm{KPa}$ and a ten times increase $k_{1M} = 23.6\,\mathrm{KPa}$ of the fiber stiffness accordingly. We repeated all previous calculations for the entirely softening media, the media without softening, the case where the matrix does not soften while the fibers do, and the case where the fibers do not soften while the matrix does. Though some quantitative changes were observed as compared to Fig. 6 the qualitative conclusion remains the same: *the overall strength is controlled by the strength of the fibers*.

Then, we examined the effect of the increase $\beta_M = \pi/4$ of the fiber angle and the increase $\phi_M = 10c_M$ of the matrix failure constant accordingly. We again repeated all previous calculations for the entirely softening media, the media without softening, the case where the matrix does not soften while the fibers do, and the case where the fibers do not soften while the matrix does. Though some quantitative changes were again observed as compared to Fig. 6, the qualitative conclusion remains the same again: *the overall strength is controlled by the strength of the fibers*.

At this point our first task, the examination of the relative contribution of the matrix and fibers to the overall layer strength, is accomplished. We turn to the second task—the examination of the relative contribution of the media and the adventitia to the overall layer strength.

The pressure–displacement curve for the bi-layer arterial model including the media and the adventitia is presented in Fig. 7 for the 'ground state' of material constants described above. Evidently, two peaks on the curve correspond to the failures of the media and adventitia correspondingly. The distribution of stresses corresponding to the first peak, where media fails, is shown in Fig. 8, while the distribution of stresses corresponding to the second peak, where adventitia fails, is shown in Fig. 9.

Finally, we check how the inclusion of residual stresses, $\omega = 160^\circ$, $A = 1.43\,\mathrm{mm}$, $B_M = 1.69\,\mathrm{mm}$, $B = 1.82\,\mathrm{mm}$ affects the arterial strength as compared to the defined 'ground state'—Fig. 7. Evidently, the presence of residual stresses leads to a dramatic increase of the overall strength—Fig. 10.

4. Discussion and conclusions

A novel softening hyperelasticity model of the arterial wall was presented to allow for a description of arterial

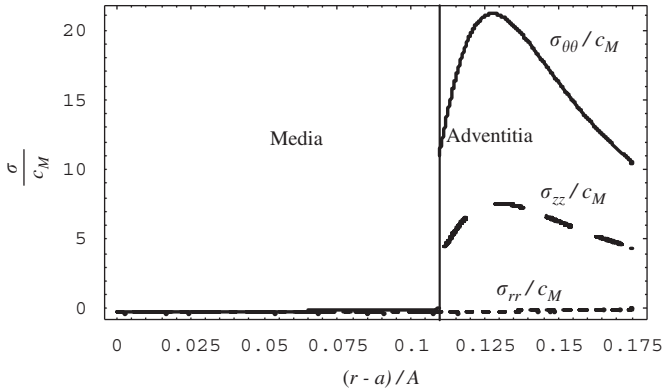

Fig. 9. Distribution of the Cauchy stresses at the point of the adventitia rupture.

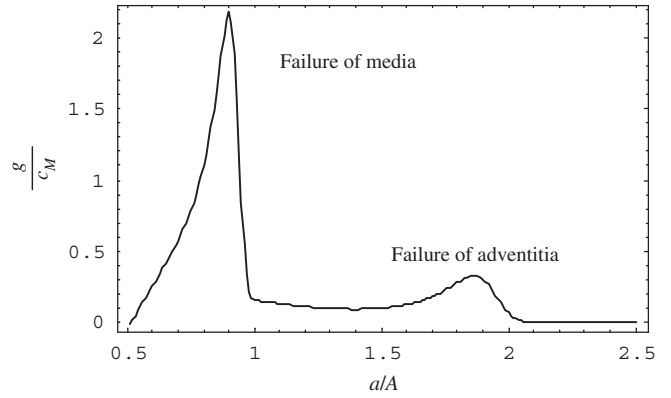

Fig. 10. Pressure–displacement curve for the 'ground state' of the bi-layer arterial wall with the residual stresses.

failure. This model includes two layers of media and adventitia. Every layer comprised the cellular matrix described by the Neo–Hookean isotropic material with softening and two families of fibers described by the exponential stored energy function with softening. The softening is controlled by one constant for the matrix material and two constants for the fiber. All these constants can be calibrated in the uniaxial tension experiments. Introduction of the new model was motivated by the necessity to give a more comprehensive failure description than the local critical stress criterion of strength of materials on the one hand and to give a simpler approach to the failure description than damage mechanics on the other hand.

Failure analysis based on the softening hyperelasticity approach allows tracking a global load–displacement path of an artery as shown in Figs. 7 and 10. The critical points correspond to the onset of instability of the static deformation path. The instability occurs when the material, media or adventitia, fails locally, i.e. the molecular bonds tear, and the local failure develops. The postcritical evolution corresponding to the decreasing branches on the load–displacement curve requires, generally, a dynamic consideration. The dynamic jump between the stable branches of the intact media and adventitia resembles the classical snap-through buckling of thin-walled structures. The use of the softening hyperelasticity for the dynamic failure propagation, however, is beyond the scope of the present work.

The proposed model was applied to the problem of the artery inflation under internal pressure. Numerical simulations led to the following three findings. Firstly, it was found that the fiber strength dominates the overall arterial strength. Such a conclusion has immediate experimental implication: it is necessary to calibrate the mechanical models of individual fibers in order to predict the global arterial strength. Of course, the role of the fiber binding energy may also be important. The latter is the reason why the experiments with the fiber bundles are of great interest too. Secondly, it was also found that the media dominates the overall arterial strength and plays the crucial role in the load-bearing capacity of arteries. Such a conclusion is in a good qualitative agreement with the fact that the rupturing aneurysms lack the media layer (Humphrey and Canham, 2000). Thirdly, it was found that residual stresses can increase the overall arterial strength significantly. The pre-existing compression in arteries delays the onset of rupture like the pre-existing compression in the pre-stressed concrete delays the crack opening. More experiments are welcome to clarify this interesting issue.

Conflict of interest

None declaired.

References

Arnoux, P.J., Chabrand, P., Jean, M., Bonnoit, J., 2002. A visco-hyperelastic with damage for the knee ligaments under dynamic constraints. Computer Methods in Biomechanics and Biomedical Engineering 5, 167–174.

Buehler, M.J., 2006. Large-scale hierarchical molecular modeling of nano-structured biological materials. Journal of Computational and Theoretical Nanoscience 3, 603–623.

Calvo, B., Pena, E., Martinez, M.A., Doblare, M., 2006. An uncoupled directional damage model for fibred biological soft tissues. Formulation and computational aspects. International Journal for Numerical Methods in Engineering 10, 2036–2057.

Chuong, C.J., Fung, Y.C., 1983. Three-dimensional stress distribution in arteries. Journal of Biomechanical Engineering 105, 268–274.

Cowin, S.C., Humphrey, J.D., 2002. Cardiovascular Soft Tissue Mechanics. Springer, New York.

Delfino, A., Stergiopulos, N., Moore, J.E., Meister, J.-J., 1997. Residual strain effects on the stress field in a thick wall finite element model of the human carotid bifurcation. Journal of Biomechanics 30, 777–786.

Demiray, H., 1991. A layered cylindrical shell model for an aorta. International Journal of Engineering Sciences 29, 47–54.

Fung, Y.C., 1993. Biomechanics: Mechanical Properties of Living Tissues, second ed. Springer, New York.

Fung, Y.C., Fronek, K., Patitucci, P., 1979. Pseudoelasticity of arteries and the choice of its mathematical expression. American Journal of Physiology 237, H620–H631.

Hokanson, J., Yazdami, S., 1997. A constitutive model of the artery with damage. Mechanics Research Communications 24, 151–159.

Holzapfel, G.A., Gasser, T.C., Ogden, R.W., 2000. A new constitutive framework for arterial wall mechanics and a comparative study of material models. Journal of Elasticity 61, 1–48.

Holzapfel, G.A., Ogden, R.W., 2003. Biomechanics of Soft Tissues in Cardiovascular System. Springer, Wien.

Holzapfel, G.A., Ogden, R.W., 2006. Mechanics of Biological Tissue. Springer, Wien.

Humphrey, J.D., 1995. Mechanics of arterial wall: review and directions. Critical Reviews in Biomedical Engineering 23, 1–162.

Humphrey, J.D., 2002. Cardiovascular Solid Mechanics: Cells, Tissues, and Organs. Springer, New York.

Humphrey, J.D., Canham, P.B., 2000. Structure, mechanical properties, and mechanics of intracranial saccular aneurysms. Journal of Elasticity 61, 49–81.

Hurschler, C., Loitz-Ramage, B., Vanderby, R., 1997. A structurally based stress–stretch relationship for tendon and ligament. Journal of Biomechanical Engineering 119, 392–399.

Kabla, A., Mahadevan, L., 2007. Nonlinear mechanics of soft fibrous networks. Journal of the Royal Society Interface 4, 99–106.

Liao, H., Belkoff, S.M., 1999. A failure model for ligaments. Journal of Biomechanics 32, 183–188.

Natali, A.N., Pavan, P.G., Carniel, E.L., Luisiano, M.E., Taglialavoro, G., 2005. Anisotropic elasto-damage constitutive model for the biomechanical analysis of tendons. Medical Engineering and Physics 27, 209–214.

Rachev, A., Greenwald, S.E., 2003. Residual stresses in conduit arteries. Journal of Biomechanics 36, 661–670.

Raghavan, M.L., Vorp, D.A., 2000. Toward a biomechanical tool to evaluate rupture potential of abdominal aortic aneurism: identification of a finite strain constitutive model and evaluation of its applicability. Journal of Biomechanics 33, 475–482.

Rivlin, R.S., 1948. Large elastic deformations of isotropic materials, IV. Further developments of the general theory. Philosophical Transactions of the Royal Society of London A 241, 379–397.

Rodrıguez, J.-F., Cacho, F., Bea, J.A., Doblare, M., 2006. A stochastic-structurally based three dimensional finite-strain damage model for fibrous soft tissue. Journal of the Mechanics and Physics of Solids 54, 564–886.

Schechtman, H., Bader, D.L., 2002. Fatigue damage of human tendons. Journal of Biomechanics 35, 347–353.

Simon, B.R., Kaufmann, M.V., McAfee, M.A., Baldwin, A.L., 1998a. Porohyperelastic finite element analysis of large arteries using ABAQUS. Journal of Biomechanical Engineering 120, 296–298.

Simon, B.R., Kaufmann, M.V., McAfee, M.A., Baldwin, A.L., Wilson, L.M., 1998b. Identification and determination of material properties for porohyperelastic analysis of large arteries. Journal of Biomechanical Engineering 120, 188–194.

Tözeren, A., 1984. Elastic properties of arteries and their influence on the cardiovascular system. Journal of Biomechanical Engineering 106, 182–185.

Vaishnav, R.N., Young, J.T., Patel, D.J., 1973. Distribution of stresses and of strain-energy density through the wall thickness in a canine aortic segment. Circulation Research 32, 577–583.

Volokh, K.Y., 2004. Nonlinear elasticity for modeling fracture of isotropic brittle solids. Journal of Applied Mechanics, ASME 71, 141–143.

Volokh, K.Y., 2006a. Compressibility of arterial wall in ring-cutting experiments. Molecular and Cellular Biomechanics 3, 35–42.

Volokh, K.Y., 2006b. Stresses in growing soft tissues. Acta Biomaterialia 2, 493–504.

Volokh, K.Y., 2007a. Softening hyperelasticity for modeling material failure: analysis of cavitation in hydrostatic tension. International Journal of Solids and Structures 44, 5043–5055.

Volokh, K.Y., 2007b. Hyperelasticity with softening for modeling materials failure. Journal of the Mechanics and Physic of Solids, in press.

von Maltzahn, W.-W., Besdo, D., Wiemer, W., 1981. Elastic properties of arteries: a nonlinear two-layer cylindrical model. Journal of Biomechanics 14, 389–397.

Wolfram, S., 2003. The Mathematica Book, fifth ed. Wolfram Media.

Wuyts, F.L., Vanhuyse, V.J., Langewouters, G.J., Decraemer, W.F., Raman, E.R., Buyle, S., 1995. Elastic properties of human aortas in relation to age and atherosclerosis: a structural model. Physics in Medicine and Biology 40, 1577–1597.